Desalination and Water Treatment
www.deswater.com

doi:10.5004/dwt.2019.24573

165 (2019) 83–96
October

A novel approach to remove ofloxacin antibiotic from industrial effluent using magnetic carbon nanocomposite prepared from sawdust of *Dalbergia sissoo* by batch and membrane hybrid technology

Muhammad Wahab[a], Muhammad Zahoor[b,*], Syed Muhammad Salman[a]

[a]*Department of Chemistry, Islamia College University, Peshawar 25000, Khyber Pakhtunkhwa, Pakistan, email: mwahabbajaur@gmail.com (M. Wahab), salman@icp.edu.pk (S.M. Salman)*
[b]*Department of Chemistry, University of Malakand, Chakdara Dir Lower, 18800. Khyber Pakhtunkhwa, Pakistan, email: mohammadzahoorus@yahoo.com (M. Zahoor)*

Received 13 February 2019; Accepted 15 June 2019

ABSTRACT

In this research work, the removal of ofloxacin (OFL) from industrial effluents were carried out through batch and membrane hybrid process using magnetic carbon nanocomposite (MCN) prepared from waste biomass (Dalbergia sissoo sawdust). The novel adsorbent was characterized by EDX (Energy dispersive x-ray), SEM (scanning electron microscopy), XRD (X-ray diffraction), FTIR (Fourier transform infrared), and TG/DTA (Thermal gravimetric/Differential thermal analysis). The deposited Fe_3O_4 (iron oxide) on the composite surface was confirmed through XRD, SEM, and FTIR. Batch adsorption experiments were performed in order to determine the optimal condition of adsorption and effect of various experimental parameters likes pH, contact time, adsorbent dosage, initial OFL concentration and temperature on the sorption process. Langmuir, Freundlich, Temkin, Jovanovic and Harkins-Jura models were used to determine different adsorption parameters. The kinetics data were analyzed using pseudo-first and second order, power function, Natarajan and Khalaf, and intraparticle diffusion models. The best fit was obtained with the pseudo-second order kinetic model. The value of ΔH^o and ΔS^o were found to be –27.948 and 110.17 kJ/mol indicating the exothermic and spontaneous nature of the process. An increase in adsorption with increase in temperature is evident from the values of ΔG^o: –32.31, –33.41, –34.51 and –35.61 kJ/mol corresponding to 20, 30, 40, 50 and 60°C. To evaluate the effect of MCN on membrane parameters, the continuous stirred reactor was connected with UF, NF, and RO membranes. Higher % retention and improved permeate flux were obtained for MCN/UF, MCN/NF, and MCN/RO processes. The percent retention of OFL observed for MCN/UF, MCN/NF, and MCN/RO hybrid processes were 57.8, 98.9 and 99.57 respectively.

Keywords: Adsorption; Isotherms; Membranes

1. Introduction

Pharmaceutical products like antibiotics are used worldwide for the treatment of human and veterinary diseases from last 70 years [1–4]. Most antibiotics are poorly metabolized by humans and animals after injection and usually 25–75% may leave from the body in unaltered form after administration into the living bodies [5–7]. Moreover, antibiotics mixed with animal feeds are directly or sprayed on fruits and crops are released into the environment [8]. These discharged antibiotics remain biologically active for specified duration of time depending on their half life cycles and ends up in different environmental compartments [9–11]. Antibiotics like ofloxacin (OFL) degrade very slowly and remains active in soil for about 30–80 d at a temperature ranging from 20 to 30°C [12]. The main sources of OFL contamination in water bodies are industrial effluents

*Corresponding author.

and fecal contamination. The presence of antibiotics in the environment in the environment is a threat which enhances the drug resistance of microorganism towards this antibiotic [13,14].

A number techniques like photo catalytic degradation, catalytic degradation, biodegradation, ozonation, advanced oxidation, biomembranes, biological filtration, and ion exchange have been applied to remove antibiotics from waste waters [15–18]. However, most of these methods have low efficiencies and produces a large amount of sludge which limit the effectiveness of them [19–21]. Amongst them, adsorption is a simple, superior, low cost and environment-friendly method that is widely used for such type of applications [22,23]. A number of adsorbents such as silica gel, zeolites, clay, and activated carbon have been used for the removal of antibiotics from wastewater [24]. The adsorption processes involving activated carbon are superior as the fine particles of carbon materials offer a large surface area for the adsorptive removal of environmental contaminants. However, activated carbons have the difficulty of regeneration and have long settling times which limits their uses in continuous stirred reactors [25,26]. To overcome these problems activated carbons are now a days converted into magnetic nanocomposites (having magnetic character and comparable surface area) which can easily be collected from slurry after use through the application of magnet [27,28].

Membrane technology is a modern technique that has been used to remove antibiotics from wastewater [29]. Different membranes like ultra filtration (UF), reverse osmosis (RO) and nanofiltration (NF) have been utilized to prepare portable waters [30]. The transport of neutral compounds through membranes is controlled by the sieving mechanism and in the case of charge compounds, the charge exclusion plays an important role in the rejection of that particular substance by membrane. The sieving mechanism is based on molecular weight cut off (MWCO) data [31]. The pollutants present in wastewater also affect the performance of membrane processes. Based on the effect produced by contaminants on membranes, they are classified into two groups: (i) the pollutants capable of destroying the membrane and (ii) the pollutants having the ability to form scaling on membrane (fouling). Membrane fouling negatively affect the membrane efficiency. Their cleaning through various chemicals is loss of economy as well. In order to improve pollutants removal efficiencies of membranes and decrease fouling, activated carbon in combination with the UF, RO, and NF have been applied by number of researchers [32,33]. Primarily, it was considered that the activated carbon would form a spongy cake on the membrane system and will not effects the permeate flux. However, later on, it was found that this spongy cake also negatively affect the permeate flux [34]. To overcome these drawback magnetic carbon nanocomposite (MCN) have been used in combination with the membrane system by a number of authors [26–28].

MCN due to its magnetic character can easily be removed from slurry after use and thus its entry into the membrane system could be easily stopped. Thus, spongy layer formation on the membrane system would be minimized. The objectives of this research work was to prepare magnetic carbon nanocomposite, characterize and use it for the effective removal of OFL from industrial effluents through adsorption/membrane hybrid processes.

2. Experimental

The ofloxacin antibiotic (purity = 99.5%, chemicals formula ($C_{18}H_{20}FN_3O_4$), molecular weight = 361.368 g/mol, maximum wavelength (λ_{max}) = 294 nm) was obtained from Medi Craft industry Hayat Abad Peshawar, Pakistan. The waste effluents were also collected from the drainage line of this industry. The chemical structure of OFL is shown in Fig. 1. All the other chemicals were of analytical grade and obtained from BDH, Fisher, and Merck.

2.1. Preparation of magnetic carbon nanocomposite

Magnetic carbon nanocomposite was prepared from the sawdust of *Dalbergia sissoo* collected from District Bajaur, Pakistan. The dried sawdust was added to a 100 ml alcoholic solution containing ferric chloride ($FeCl_3$) and ferrous sulfate ($FeSO_4$) in 2:1 ratio. After 24 h, NaOH was added drop wise to the mixture at 70°C. The sawdust was then separated from mixture using Whattman 42 filter paper and dried in electric oven. The treated, dried sawdust was then charred and ignited in a specially designed chamber containing an electric heater, wire gauze, an inlet for N_2 gas and outlet for exhaust gases. The prepared product was then washed with HCl (0.1 M) solution and double distilled water for many times to attain neutral pH. The resulting product was dried at 70°C in an electric oven.

2.2. Characterization of MCN

MCN was characterized by EDS X-sight instrument, to study the elemental compositions. The surface texture was analyzed by scanning electron microscope (SEM) at set up voltage of 10 KV. For functional group determination, Fourier Transformed Infrared FTIR (Perkin Elmer FTIR) was used (ranging from 450 to 4,000 cm^{-1}). The thermogravimetric and differential thermal analysis (TG/DTA) was carried out with diamond series (Perkin Elmer, US) analyzer using alumina as a standard. X-ray diffraction (using Nickel filter CuKα monochromatic radiations having wavelength 1.5418) analysis was performed at room temperature, current of 30 mA and voltage of 40 KV. The scanning range was 2θ/θ while scanning speed was 10 min^{-1}. Surface area and pore distribu-

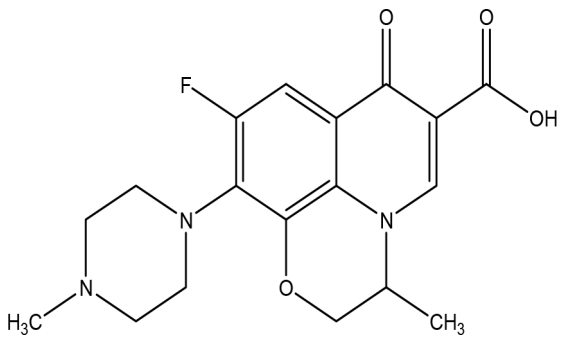

Fig. 1. Structure of ofloxacin.

tion of MCN was measured using Quantachrome pore surface area and size analyzer (NOVA, 2200e, USA).

2.3. Batch adsorption experiment

The effect of various physicochemical parameters like pH, contact time, initial OFL concentration, adsorbent dose, and temperature on OFL adsorption on MCN were evaluated using batch experiments. Working standard OFL solutions of different concentrations were prepared by diluting OFL stock solution with double distilled water. The solution pH was adjusted using 0.1 M HCl and NaOH solutions. In 250 ml Erlenmeyer flasks containing 50 ml solutions of the required concentrations were contacted with 0.1 g adsorbent (except for the investigation of adsorbent dose) in all experiments and kept in a rotary shaker at 170 rpm for a specific interval of time. All the experiments were carried out in triplicate and their mean values are presented. The MCN was removed from solution through a bar magnet and then through Whattman no 42 filter paper. Filtered samples were analyzed by UV visible T-60 spectrophotometer for ofloxacin remaining concentrations at 298 nm.

The amount of OFL adsorbed q_e (mg/g) and percent removal (% R) was calculated using the following equations [35–37].

$$q_e = \left(C_i - C_f\right) \times \frac{V}{m} \tag{1}$$

$$\%R = \frac{\left(C_i - C_f\right)}{C_i} \times 100 \tag{2}$$

where C_i is initial OFL concentration in mg/L, C_f is final OFL concentration in mg/L, V volume of OFL solution in L and m is mass of adsorbent in g.

2.4. Adsorption kinetics

For the determination of kinetics parameters of OFL adsorption on MCN, a specified amount of adsorbent (0.1 g) was mixed with known volumes of 30 and 80 mg/L OFL solutions. The solutions were shaken for 240 min at a speed of 170 rpm. Pseudo-first and second order, Elovich, Power function, Natarajan and Khalaf, and intraparticle diffusion models were applied to analyze the kinetics experiment data.

2.5. Isothermal studies

The effect of OFL concentration on MCN was studied at room temperature. Known volumes (50 mL) of specified concentration (20 to 200 mg/L) solutions of OFL were contacted with 0.1 g of adsorbent. Their q_e values were determined from Eq. (1) and plotted against equilibrium concentration. Langmuir, Freundlich, Temkin, Jovanovic and Harkin-Jura models were applied to analyze the adsorption equilibrium data.

2.6. Thermodynamic study

The effect of temperature on OFL adsorption on MCN was studied at 20, 30, 40, 50 and 60°C keeping other parameters constant (volume = 50 mL, concentration = 80 mg/L, adsorbent dose = 0.1 g, pH = 6, shaking time = 2 h, shaking speed = 170 rpm). For every temperature, 50 mL OFL solution (80 mg/L) was contacted with 0.1 g of adsorbent and shaken at 170 rpm for two hours. The remaining amount of OFL left in solution after adsorption were determined using UV/visible T-60 spectrophotometer.

2.7. Effect of pH and adsorbent dose

The effect of pH on OFL adsorption was studied in the range of 2–12. The solution pH was adjusted by using 0.1 M HCl, and NaOH solutions. Different pH solutions containing specified amount of OFL were contacted with 0.1 g of adsorbent in flasks for 2 h and shaken at 170 rpm. The OFL concentration after adsorption were determined using UV/visible T-60 spectrophotometer.

The effect of adsorbent dosage on OFL adsorption was studied from 0.01 to 0.15 g. Other parameters were similar as mentioned above. To different flasks containing 50 mL of OFL solutions different amount of adsorbent (0.01–0.15 g) were added and shaken for 2 h at 170 rpm. The remaining concentration of OFL in the supernatant were determined using UV/visible T-60 spectrophotometer.

2.8. Removal of OFL by membrane technology

Three different membranes; UF, RO and NF were used to filter industrial wastewater effluents containing OFL. The percent retention of OFL by the selected membranes were determined from the concentration differences between the bulks and permeate (determined through UV/visible T-60 spectrophotometer). The effect of OFL on permeate fluxes through the membranes were determined from the differences of flow meters installed at the in and out of the membrane pilot plant.

The percent retention was determined using the formula:

$$\%R = \left(1 - \frac{C_p}{C_b}\right) \times 100 \tag{3}$$

where C_p and C_b (mg/L) are concentrations of OFL in permeate and bulk feed respectively. The permeate flux (J) was calculated using the equation:

$$J = \frac{1}{A} \times \frac{dv}{dt} \tag{4}$$

where A is the surface area of the membrane (m^2), V volume of permeate (L) and t is filtration time (h). The backwashing of each membrane was performed after each experimental cycle.

The characteristics of the membranes used in this study are listed in Tables 1–3. Membranes were initially washed with double distilled water according to manufacturer provided information. A solution of 80 mg/L was prepared in double distilled water. All the required samples were retained to room temperature, neutral pH and transmembrane pressure was 1 bar in all experiments. The % rejection of OFL and the consequent decrease in the permeate flux were determined as mentioned above.

Table 1
UF membrane parameters

Parameters	Specification
Membrane polymer	Polyether sulfone
Membrane type	Capillary multi bore × 7
Diameter bore ID, mm	0.9
Fiber inside diameter range, mm	4.2
MWCO, kD	100
Membrane area, m^2	50
Maximum operating temperature, °C	40
Maximum pressure, bar	7.5
Membrane backwash pressure, bar	0.5–1
pH operating range	3–10
Back wash pH operating range	1–13
Disinfection chemicals	
Hypochloride (NaOCl), mg/L	50–200
Hydrogen per oxide (H_2O_2), mg/L	100–200

Table 2
RO membrane parameters

Parameters	Specification
Manufacture	Dow Film Tech
Model	RO (270–2540)
MWCO	200
Membrane	Thin film composite
Permeate flow rate	850 gal/D (3.2 m^2)
Membrane surface area	28 ft^2 (3.2 m^2)
Maximum operating pressure	1.0 bar
Stabilized salt rejection	99.5%
pH operating range	3–10
pH range short term cleaning	1–12

Table 3
NF membrane parameters

Parameters	Specifications
Manufacturer	Dow Film Tech
Model	NF 270–2540
MWCO	200–300
Permeate flow rate	850 gal/D (3.2 m^3/d)
Membrane surface area	28 ft^2 (3.2 m^2)
Applied pressure	4.8 bar
Stabilized salt rejection	> 97%

2.9. Adsorption/Membrane hybrid processes

In order to enhance the membrane efficiencies, the adsorption and membrane processes were combined in a hybrid manner for which a pilot plant was devised. About 8 L solutions of 80 mg/L concentration of OFL was prepared in double distilled water and passed through UF, RO and NF membranes using an electric water pump. The percent retention of OFL by the membranes and their subsequent effect on permeate fluxes were noted. The membranes were then used in a hybrid manner with continuous stirred reactor containing MCN, where OFL solution was contacted with MCN for about 2 h before passing through membranes. The UF membrane was operated in dead-end mode while the NF and RO membranes in cross flow mode. A particularly designed container equipped with the electromagnetic arrangement was placed in the pilot plant for MCN separation after use in order to prevent its entry into membrane system and consequently avoid the formation of spongy cake layer over the membrane surface which would otherwise have to effect the efficacy of membrane. The membrane parameters such as percent retention and permeate fluxes for MCN/UF, MCN/RO, and MCN/NF were determined.

2.10. Regeneration of adsorbent

About 0.1 g of adsorbent was mixed with 50 mL of OFL (80 mg/L) solution (pH 6) at room temperature and shaken at 170 rpm for 4 h. The adsorbent was then separated from slurry through magnet, washed with 5% NaOH solution, methanol and then with distilled water five times. Then it was oven dried at 70°C for 2 h. The adsorbent was then used and regenerated up to 6 cycles and the decrease in removing OFL efficiency was noted.

3. Results and discussions

3.1. Characterization of MCN

The magnetic nanocomposites were prepared from *Dalbergia sissoo* sawdust. The magnetic property of the adsorbent was checked with a magnet bar. The prepared MCN completely adhered to the magnet which confirmed the magnetic character of the sample.

The elemental diffraction X-ray of MCN is shown in Fig. 2a. The figure shows the presence of carbon, iron and oxygen peaks. Small peaks of calcium, magnesium and potassium (impurities) were also observed.

The SEM images are shown in Figs. 2b–d, reflecting the surface morphology and texture of MCN. The images shows a clear irregular shaped composite particles with crooks and shattered edges suggesting to be a suitable surface for adsorption. The dots like structures on the surface shows iron oxide (Fe_3O_4). SEM images also show the cubic crystalline structure of iron oxide deposited on MCN.

Figs. 2e and f, shows FTIR spectra of MCN with characteristic peaks. The peak from 2250–2300 cm^{-1} presenting C≡C while the peak from 3200–3400 cm^{-1} indicating O-H group. The peaks between 1700–1800 indicating anhydride and aldehydes groups while the characteristic peak at 700 shows the Fe-O bond. The shifting in peaks as shown in graph 2f confirms the adsorption of OFL on MCN.

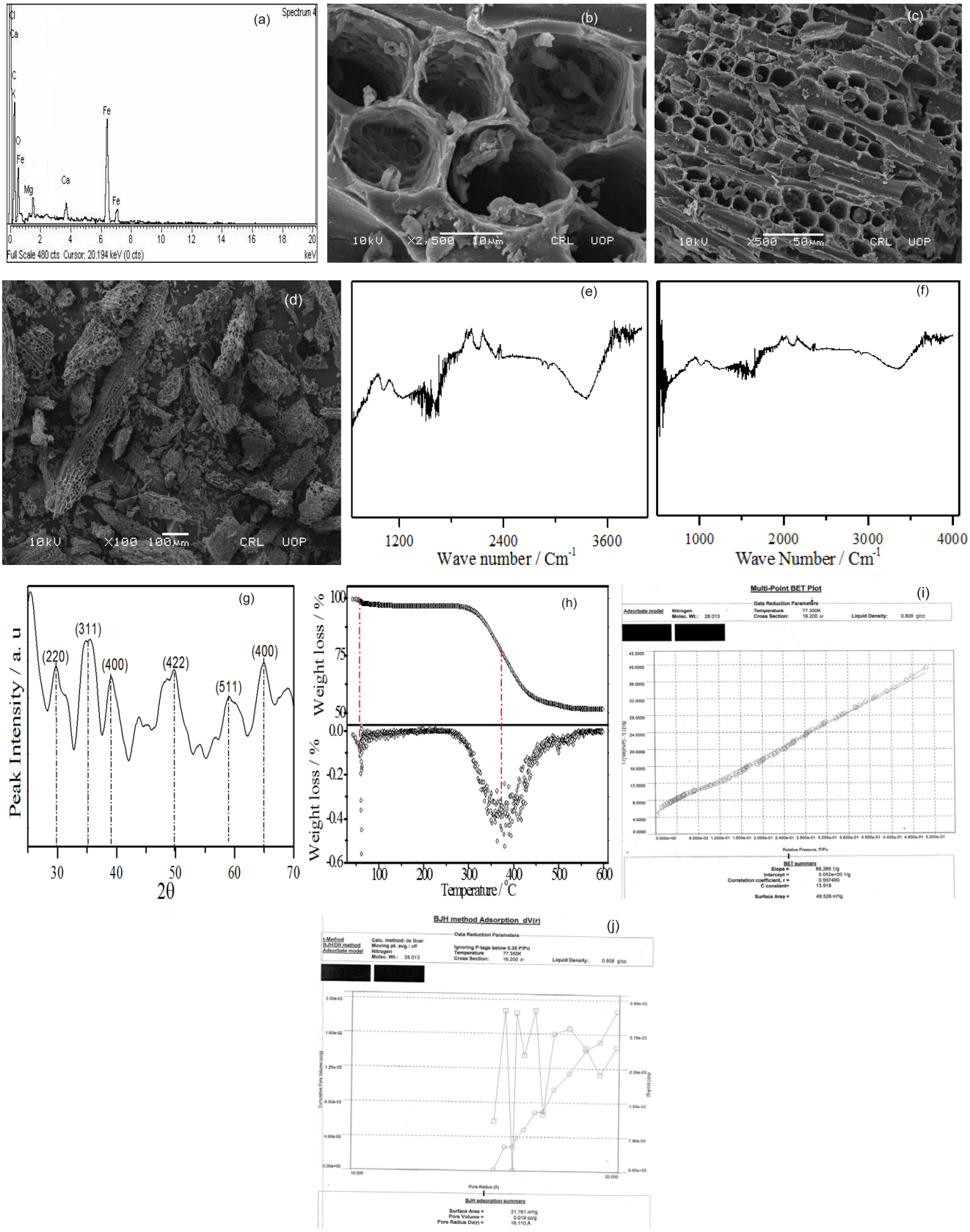

Fig. 2. Instrumental characterization of MCN.

XRD is a technique used to determine the crystal structure and particle size. Fig. 2g suggests a crystalline structure of iron oxide deposited over the carbon surface. The peaks observed at 2θ values of 29, 36, 38 and 50 corresponding to indices planes of 220, 311,400 and 422 representing magnetite. The presence of magnetite and maghemite are important for an adsorbent to have magnetic character [26–28].

The TG/DTA of the MCN is given in Fig. 2h. The initially, a mass of 5.663 g of MCN was taken. From 0 to 60ºC, the observed mass loss was 3% which was due to water evaporation. Up to 318ºC, the second mass loss of about 7% was observed which was due to thermal degradation of cellulose material. The third mass loss of 58% was observed above 318ºC which was attributed to the formation carbonaceous residues and phase transition from Fe_3O_4 to FeO.

The BET and BJH surface area micro graph are shown in Figs. 2i and j. The BET, BJH surface area, pore volume, pore radius were found to be 49.526 m^2/g, 21.761 m^2/g, 0.019 cc/g, and 16.110 A^o respectively.

3.2. Isothermal studies

The adsorption of OFL on MCN was studied for a wide concentration range of OFL (20–200 mg/L). With the increase in concentration, there was an increase in the adsorption of OFL. Various Isotherm models such as Langmuir, Freundlich, Temkin, Jovanovic and Harkins-Jura were used to determine the isotherm parameters and explain the observed adsorption behavior.

3.2.1. Langmuir adsorption isotherm

Adsorption phenomenon are generally explained through graph known as adsorption isotherms (Fig. 3a). Usually, adsorption of adsorbate on the adsorbent is a function of concentration at a given temperature. The Langmuir isotherm is about mono layer adsorption on to a surface containing a finite number of adsorption sites of uniform diameters with no transmigration of adsorbate on the surface. Once a site is occupied no further adsorption takes place on that site. This means that the when surface reaches to a saturation point, maximum adsorption is achieved. The linear form of Langmuir isotherm is given as follows [38].

$$\frac{C_e}{q_e} = \frac{1}{K_L q_m} + \frac{C_e}{q_m} \tag{5}$$

where q_e represent the amount of adsorbate adsorbed at equilibrium (mg/g), C_e represents adsorbate concentration at equilibrium (mg/L), q_m represent maximum removal capacity of adsorbate by adsorbent (mg/g), b is an empirical constant relating to energy of adsorption. C_e/q_e vs C_e plot of OFL is shown in Fig. 3b. q_m and b were calculated from slope and intercept of the plot and are presented in Table 4.

3.2.2. Freundlich adsorption isotherm

The Freundlich adsorption isotherm is an empirical equation that describes the heterogeneous system. The linear form of the Freundlich equation is given as follows [39].

$$\ln q_e = \log K_F + \frac{1}{n} \ln C_e \tag{6}$$

In Eq. (6), q_e is the amount of OFL adsorbed per unit mass of adsorbent (mg/g), K_F is adsorption capacity of adsorbent in L/mg while $1/n$ is adsorption intensity. K_F and n are Freundlich constant and were calculated from the slope and intercept of adsorption plot OFL on MCN (Fig. 3c). The values of the constants are presented in Table 4.

3.2.3. Temkin adsorption isotherm

The Temkin adsorption isotherm correlates the heat of adsorption with the surface coverage. The linear form of this isotherm is given as follows [40].

$$q_e = \beta \ln \alpha + \beta \ln C_e \tag{7}$$

where β = RT/b, R is a general gas constant and its value is 8.314 J/mol·K, T is absolute temperature (K), b is constant and related to the heat of adsorption. From q_e (mg/g) vs. ln C_e (mg/L) plot (Fig. 3d), the values of the slope β and intercept βlnα, were calculated and are presented in Table 4.

3.2.4. Jovanovic adsorption isotherm

This model of adsorption was introduced by Jovanovic. The Jovanovic isotherm is nearly similar to Langmuir isotherm. However it also considers the possibility of some mechanical interactions between the adsorbent and adsorbate. The linear form of Jovanovic isotherm is given as follow [41,42].

$$\ln q_e = \ln q_{\max} - KJC_e \tag{8}$$

where q_e represents the amount of adsorbate adsorbed per unit mass of adsorbent (mg/g), q_{max} maximum removal capacity of OFL obtained from the intercept of the graph, C_e equilibrium concentration (mg/L). The plot of lnq_e verses C_e is shown in Fig. 3e. The value of K_J and q_{max} were calculated from the slope and intercept of the plot (Table 4).

3.2.5. Harkins-Jura isotherm

Harkin-Jura isotherm considers multilayer adsorption possibility on the adsorbent surface having heterogeneous pore allocations. The linear form of the Harkins-Jura isotherm can be given as follow [43].

$$\frac{1}{q_{e^2}} = \frac{B_H}{A_H} - \frac{1}{A_H} \log C_e \tag{9}$$

where B and A are Harkins-Jura constant that can be obtained by plotting $1/q_e^2$ vs. $logC_e$ (Fig. 3f).

3.3. Kinetic study

Adsorption kinetics are very important from an economical point of view in industrial processes. The effect of contact time on adsorption of OFL on MCN for two constant initial concentrations (30 and 80 mg/L) are graphically shown in

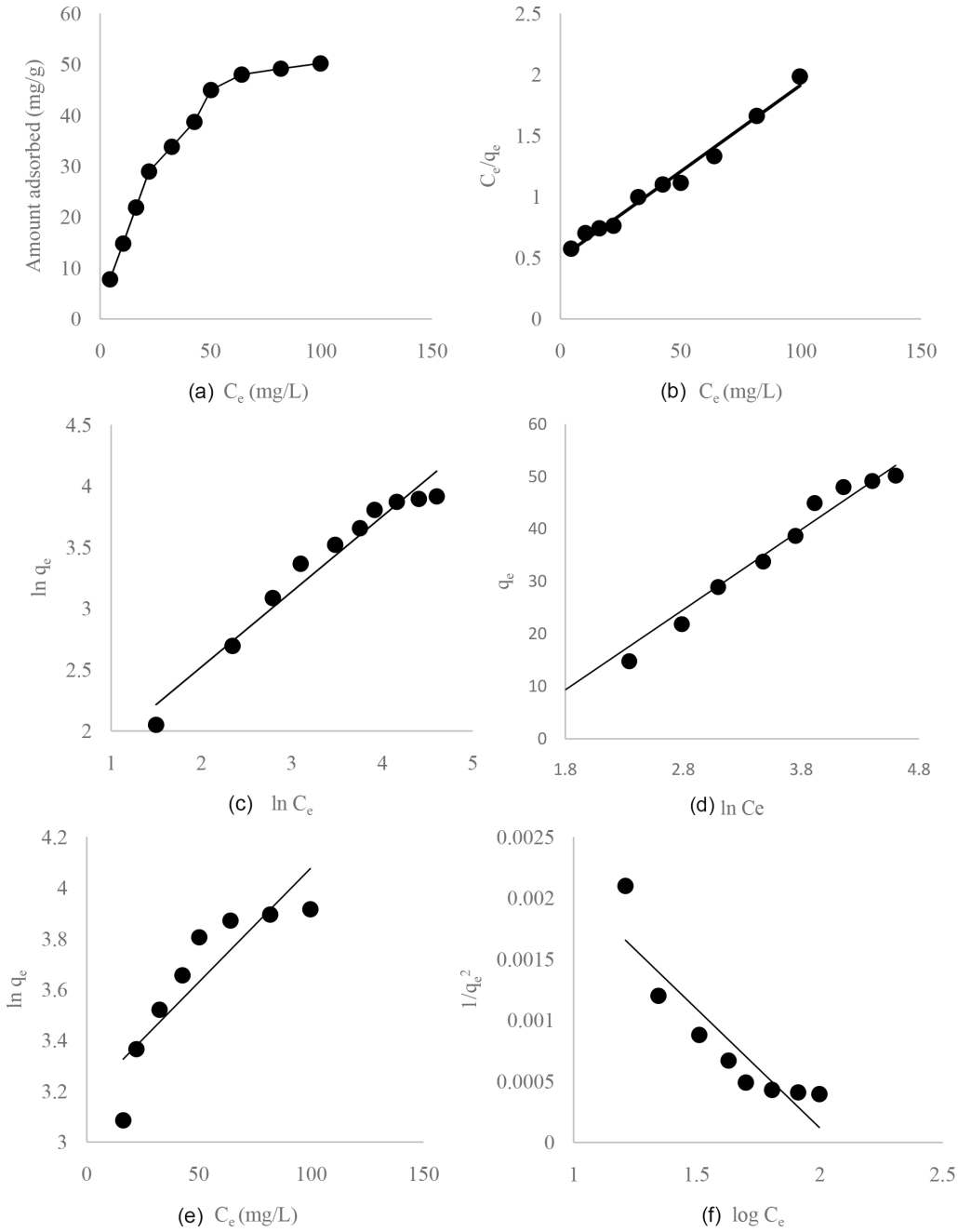

Fig. 3. Adsorption isotherms and effect of OFL concentration on adsorption. (a) Effect of concentration on adsorption of MCN (b) Langmuir plot (C) Freundlich plot (d) Tempkin plot (e) Jovanic plot (f) Harkins-Jora plot.

Fig. 4a. It is evident from the graph that as shaking time increases the removal of OFL for both concentrations were also increased. Up to 30 min a rapid increase in the removal of OFL was observed, followed by comparatively slow removal phase up to 90 min and then the equilibrium was achieved up to 120 min. The initial rapid increase was due to the existence of more binding sites, however when the binding sites get occupied then the adsorption process becomes slower. When the shaking time was increased further from 120 to 240 min, the increase in removal efficiency was negligible.

Various kinetic models such as Lagergren pseudo first and second order, power function, Natarajan and Khalaf, and intra particle diffusion were used to calculate the adsorption kinetic parameters. The mathematical forms of these models are given as follows:

Pseudo-first-order equation [44].

$$\ln\left(q_e - q_t\right) = \ln q_e - K_1 t \tag{10}$$

Pseudo-second order equation [45].

$$\frac{t}{q_t} = \frac{1}{K_2 q_{e^2}} + \frac{t}{q_e} \tag{11}$$

Table 4
Isothermal parameters for adsorption of OFL on MCN

Langmuir isotherm	
q_{max} (mg/g)	70.423
K_L (L/mg)	0.0286
R^2	0.985
Freundlich isotherm	
K_F (mg/g)	3.652
$1/n$	0.6144
R^2	0.959
Tempkin isotherm	
B	15.27
α	3.280
b	159.52
R^2	0.977
Harkins-Jura isotherm	
AH (g^2/L)	0.526
BH (mg^2/L)	2.105
R^2	0.818
Joanovic isotherm	
K_J (L/g)	–0.009
q_{max} (mg/g)	24.042
R^2	0.775

Power function kinetic equation [46].

$$\log q_t = \log a + b \log t \tag{12}$$

Natarajan and Khalaf kinetic equation [47].

$$\log\left(\frac{C_o}{C_t}\right) = \frac{K_N}{2.303} t \tag{13}$$

Intra particle diffusion model [48].

$$q_t = K_{diff} t^{1/2} + C \tag{14}$$

In Eq. (10), q_e (mg/g) is the OFL amount adsorbed per unit mass of adsorbent at equilibrium time, q_t is the OFL amount adsorbed at specific time t, K_1 (1/min) is the rate constant. The value of q_e and K_1 were calculated from the slope and intercept of plotting $ln(q_e–q_t)$ verses time plot (Fig. 4b) and are given in Table 5.

In Eq. (11), K_2 (g/mg·min) is the rate constant of pseudo-second order kinetic model. The values of q_e and K_2 were calculated from the slope and intercept of t/q_t vs time plot (Fig. 4c) and are given in Table 5.

In Eq. (12), the constant 'a' represents the initial rate and refers to the intercept of the graph, the constant 'b' represents the reaction rate and refers to the slope of the graph. By plotting $log\ q_t$ versus $log\ t$ the values of a and b were calculated (Fig. 4d) and are given in Table 5.

In Eq. (13), C_o (mg/L) represent the concentration at zero time and C_t (mg/L) represent the concentration at time t. by plotting $log(C_o/C_t)$ versus t the value of slope K_N was calculated as shown in Fig. 4e and are given in Table 5.

In Eq. (14), q_t (mg/g) is the amount of OFL adsorbed per unit mass of adsorbent at a specific interval of time. By plotting q_t versus $t^{1/2}$ the values of K_{diff} and C were calculated from the slope and intercept of the graph (Fig. 4f) and are given in Table 5. The Weber's intra particle diffusion model is usually used to determine the adsorption mechanism. Using this model one can decide whether film diffusion or intra particle diffusion is the rate limiting step. If q_t vs. $t^{1/2}$ plot is linear and passes through the origin then the intra particle diffusion is the sole rate limiting step. If the curve have multi linearity then the process is controlled more than one mechanism. The curve in Fig. 4f is multilinear and have three phases: a. the initial steep phase representing surface diffusion, b. the second less steep portion presenting gradual sorption of ofloxacin where intra particle diffusion within the pores is rate limiting and c. the third portion is somewhat linear to x-axis where equilibrium has reached. Since the curve do not passes through the origin thus intra particle diffusion is not rate limiting step and the process is controlled by more than one mechanism. There were three steps involved in sorption of ofloxacin on prepared nanocomposite, however only one predominate at a given time phase. The low values of C (Table 6) suggested that surface diffusion not playing a significant role in the rate controlling step in the overall process of sorption.

3.4. Thermodynamic studies

To determine the thermodynamic parameters of the of OFL adsorption on the prepared nanocomposite, the adsorption experiments were carried out at different temperature (20, 30, 40, 50, and 60ºC). The Vant Hoff equation was used to calculate ΔH° and ΔS° [49].

$$\ln K = \frac{\Delta S^\circ}{R} - \frac{\Delta H^\circ}{RT} \tag{15}$$

In Eq. (15), K is a constant relating to the amount of OFL adsorbed per unit mass of MCN. ΔS° presents the change in entropy while ΔH°, the change in enthalpy. R is universal gas constant and its value is 8.314 kJ/mol and T is the temperature in Kelvin.

The value of ΔH° and ΔS° were calculated by plotting $lnK\ vs.\ 1/T$ (Fig. 5a). The values of ΔH° and ΔSº were found to be –27.948 and 110.17 kJ/mol respectively pointing towards the exothermic and spontaneous nature of the process.

The values of ΔG° (Gibbs free energy change) at different temperatures were calculated using the following relation.

$$\Delta G^\circ = \Delta H^\circ - T\left(\Delta S^\circ\right) \tag{16}$$

The values of ΔG° calculated were: –32.31, –33.41, –34.51 and –35.61 corresponding to temperatures: 20, 30, 40, 50 and 60ºC. The negative values of ΔG° presenting the favorable and spontaneous nature of the process. With the increase in temperature there is an increase in ΔG° showing that the sorption of OFL increases with increase in temperature.

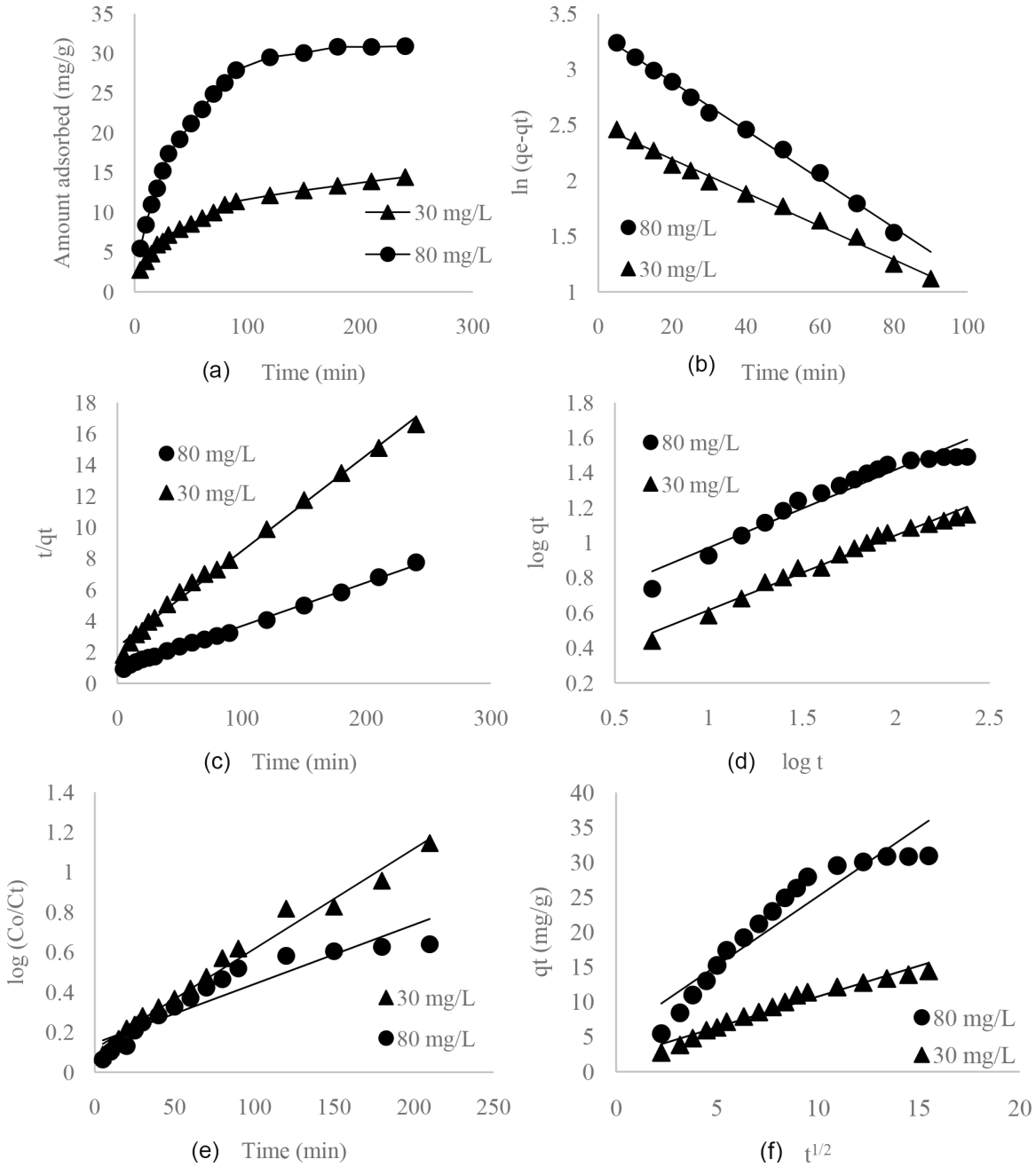

Fig. 4. Adsorption kinetics of OFL adsorption on MCN (a) Kinetics plot (b). Pseudo-first order kinetic plot (c). Pseudo second kinetic plot (d). Power function kinetic plot (e) Natarajan and Khalaf kinetic plot (f). Intra particle diffusion plot.

3.5. Effect of pH on OFL removal

The pH of the medium is an important factor that influence the sorption of any contaminants by an adsorbent. In this study the solution pH have been varied between 2 to 12 in order to investigate the effect of pH on OFL removal by MCN (Fig. 5b). The effect of pH from 2 to 6 was more significant and within this limit there was an increase in sorption of OFL. Above pH 6 there was a decrease in the sorption process. To explain the increase/decrease of sorption process, speciation curves of OFL was constructed (Fig. 5c). At low pH in acidic media (up to pH 2) OFL is neutral, while from pH 2 to 4 the predominant charge is negative on OFL molecule while from pH 4 to 6 OFL molecule has a net positive charge. The high adsorption capacity of MCN at pH 6 can be explain on the basis of favorable interactions between the adsorbent and adsorbate. The FTIR analysis showed that the adsorbent possesses a net negative charge while from pH 4 to 6 there is a net positive charge on OFL leading to favorable interaction resulting in sorption of OFL [49–51]. From pH 6 to 8 the OFL molecule is in zwitterion form which is equivalent to neutral molecule therefore, low sorption of OFL was observed. It was concluded that in anionic and neutral form the sorption of

Table 5
Kinetic parameters for OFL adsorption on MCN

Concentration (mg/L)	Rate constant		Correlation coefficient
Pseudo-second order model	K_2 (g/mg min)	q_e (mg/g)	R^2
30	0.0016	16.287	0.995
80	0.00088	35.842	0.998
Pseudo-first order model	K_1 (1/min)	q_e (mg/g)	R^2
30	0.015	12.079	0.992
80	0.0218	27.799	0.996
Power function model	a	b	R^2
30	1.541	0.4275	0.980
80	3.349	0.4465	0.942
Natarajan and Khalaf model	K_N (1/min)		R^2
30	0.0069		0.973
80	0.0115		0.983
Intraparticle diffusion model	K_{diff} (mg/g min$^{1/2}$)	C	R^2
30	0.8788	0.9809	0.966
80	1.9768	5.3583	0.892

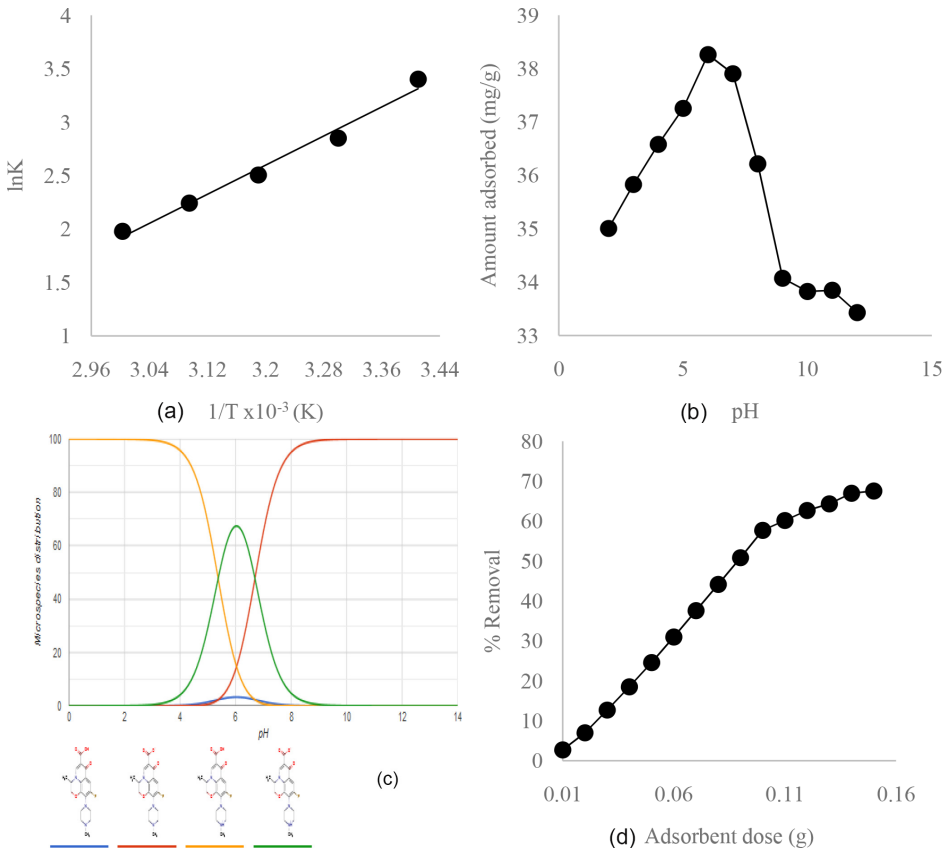

Fig. 5. Effect of temperature, pH and adsorbent dosage on adsorption of OFL a. Vant Hoff plot b. effect of pH c. speciation graph d. effect of adsorbent dosage.

OFL was relatively low while in the cationic state it was high; hence an appreciable amount of OFL was removed from solution pH 4 to 6. Above pH 6, the zwitterionic and anionic state of OFL are dominant leading adsorbent-adsorbate repulsions and thus a decrease in removal efficiency of OFL can be observed [52].

3.6. Effect of adsorbent dose

In order to determine the effect of adsorbent dosage on the removal of OFL by MCN, the MCN dosage was varied from 0.01 to 0.15 g (Fig. 5d). The removal of OFL increases with increase in MCN dosage up to 0.09 g and then remained almost constant. This increase occurred because the sorption is a surface phenomenon and with increase in surface area due to addition of adsorbent mass resulted in high sorption capacities. Further, increase in the MCN dosage leading to a competition between the adsorbent particles for adsorbate and the sorption of OFL on active sites was not effected with increase in dosage of MCN above 0.09 g [53].

3.7. Effect of OFL on permeate flux of UF, NF and RO membrane

From Figs. 6a–e, it is obvious that there was a decline in permeate flux in the early phases for distilled water when passed through all the three selected membranes, which were due to the interaction of ions present in water and also due to intrinsic membrane resistance. In distilled water gen-

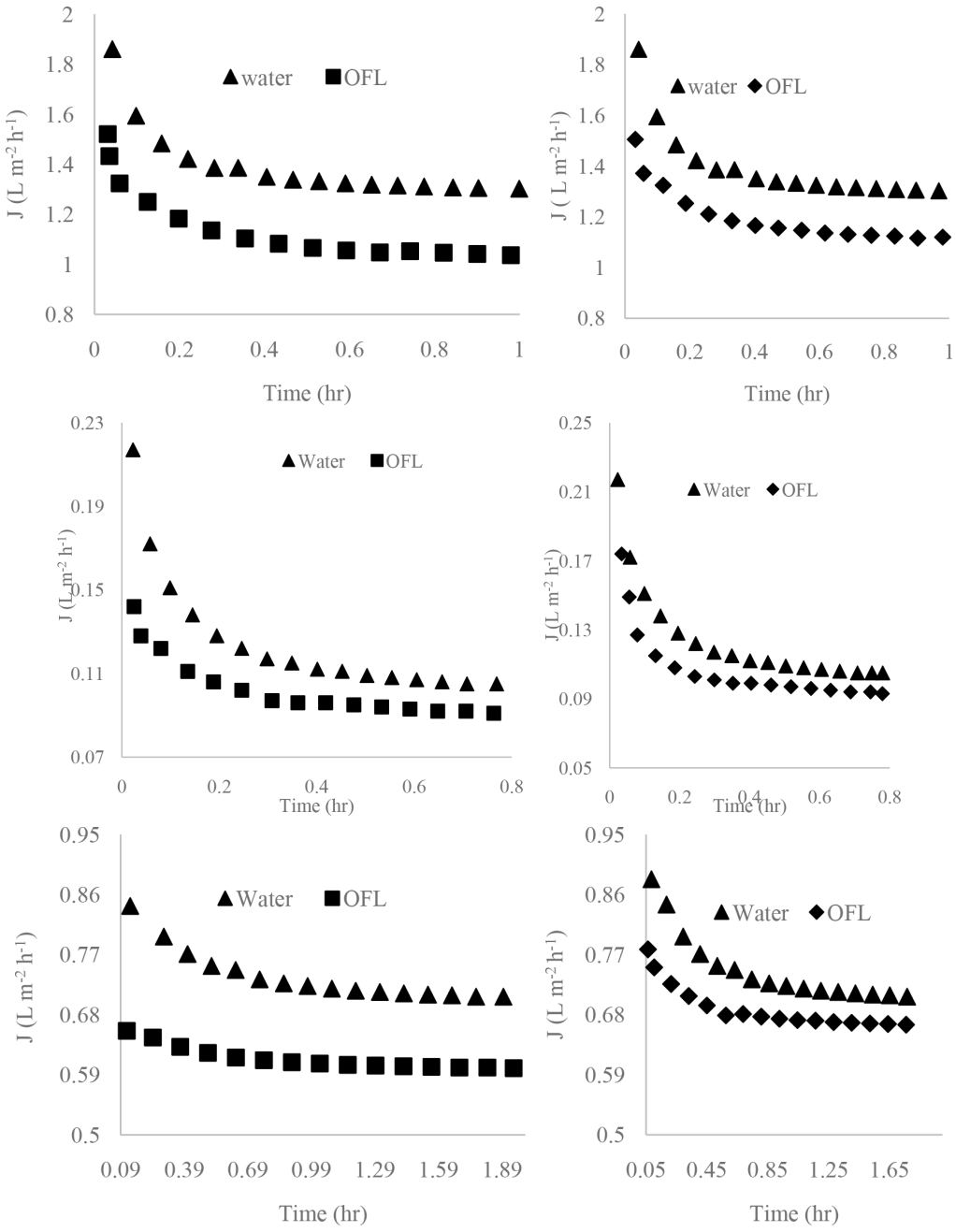

Fig. 6. Effect of OFL on membrane permeate flux and improvement brought about by MCN a. UF membrane alone b. MCN/UF c. NF membrane alone d. MCN/NF e. RO membrane alone f. MCN/RO.

erally, H^{+1} and OH^{-1} ions are present. The presence of ions is understandable from the conductance measurement (6.3×10^{-6} s m^{-1}).

The permeate flux then became steady and were not much affected within the experimental conditions and time. The adsorption of the OFL on membrane up to some extent blocks the membrane pores and results in low permeate flux.

The molecular mass of OFL is smaller than that of UF membrane MWCO. OFL molecules were expected to pass without any resistance and the concentration of permeate (C_p) water must be equal to that of bulk concentration (C_b). However, in spite of low retention, flux decline was observed for UF membrane. An improvement in permeate flux for UF/MCN process was observed (Fig. 6b).

In the case of NF and RO the molecular mass of OFL antibiotic was greater than the MWCO of these membranes which drastically affects the permeate flux. This effect of OFL antibiotic on permeate flux of NF (Figs. 6c and d) and RO (Figs. 6e and f) was more pronounced as compared that UF membrane. When NF and RO membranes were used in hybrid manner with MCN, improvement in permeate fluxes were observed.

The percent retention of OFL by the selected membranes alone and with the MCN have been presented in Fig. 7. As mentioned earlier the MWCO of UF membrane was higher than molecular weight of OFL and was expected to pass freely from UF membrane. However due to adsorption on membrane surface and concentration polarization still there was 15–20% retention of OFL. The decline in permeate flux of UF membrane was due to this retention. When the MCN pretreatment was applied the percent retention was improved from 40 to 50% and consequently improved flux was also observed (Fig. 7a). The percent retention OFL by NF and RO membranes were about 95 and 99.6% (Figs. 7 b and c) as a result the effect on permeate flux was more drastic. When these membranes were connected to the reactor where pretreatment of MCN adsorption was applied the percent retention of OFL was improved to 100% and permeate luxes were also improved.

3.8. Regeneration experiments

From economical point of view the regeneration and recycling of an adsorbent is very important as this on one hand reduces cost of a process and on another hand prevent the sludge formation. After first regeneration cycle, the initial removal capacity of OFL dropped up to 8% of the

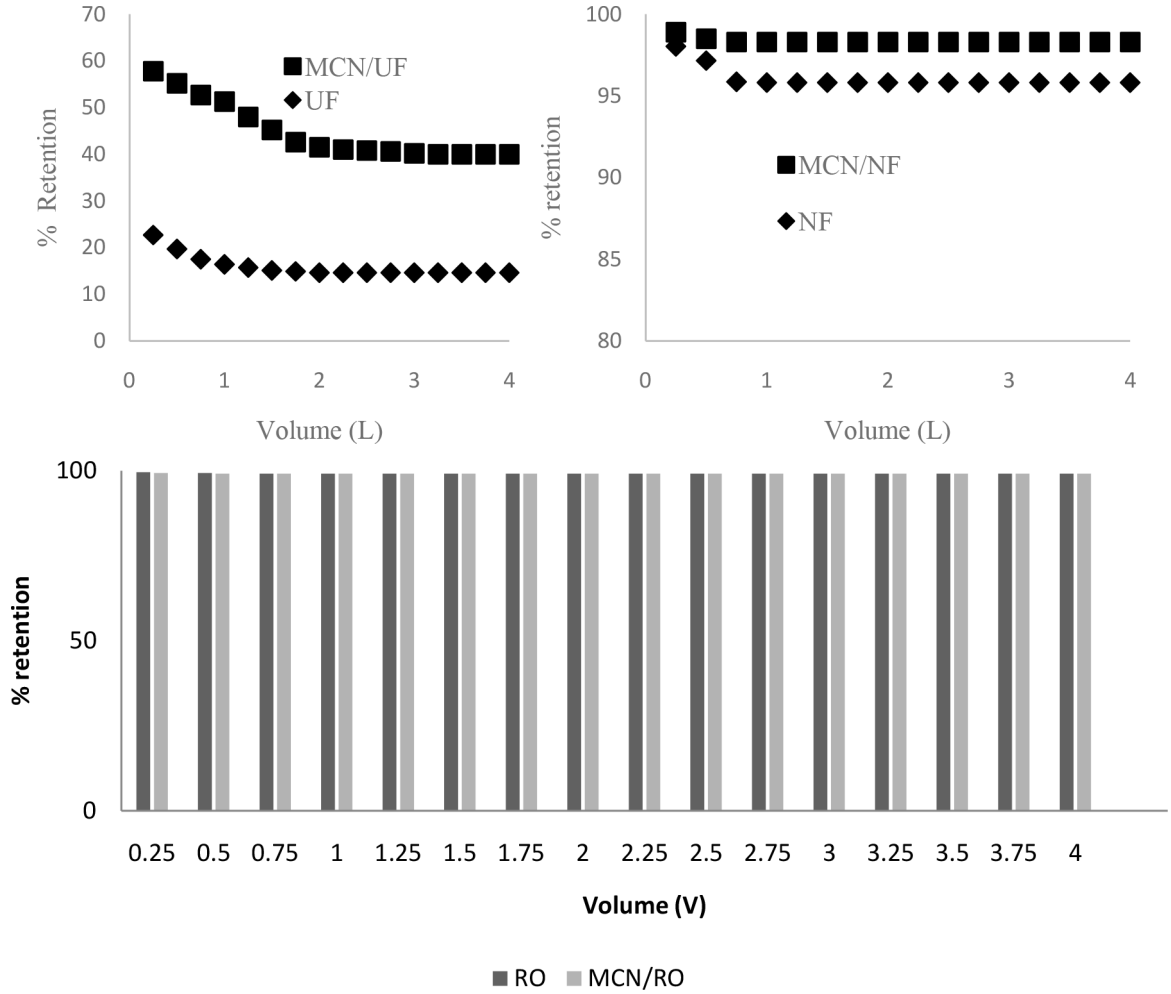

Fig. 7. Percent retention of OFL by membranes a. UF membrane b. NF membrane c. RO membrane.

original capacity and after 6th regeneration cycle the drop was 45%. From the results it can be concluded that MCN is a stable and excellent adsorbent for the removal of OFL that can easily be regenerated with minimum loss in its adsorption capacity.

4. Conclusion

In this research work, MCN was prepared from *Dalbergia sissoo* sawdust and was characterized by surface area analyzer, SEM, FTIR, XRD, EDX and TG/DTA. The magnetic character of MCN was confirmed from XRD and FTIR analysis. The MCN was tested for the removal of OFL from wastewater through batch and membrane hybrid method. MCN was found efficient in the removal of OFL from wastewater and its adsorption capability was mainly dependent on initial pH, adsorbent dose, contact time, initial OFL concentration and temperature. Best fit of the isotherm experimental data was obtained with Langmuir isotherm with R^2 value of 0.985. Kinetic studies showed that the experimental data fitted well to pseudo-second order equation with R^2 = 0.998. In membrane hybrid technology, the percent retention of OFL by UF/MCN was improved from 15 to 50% and permeate flux was also improved to some extent. In the case of NF/MCN improvement in percent retention and permeate flux was enhanced by MCN. In the case of RO/MCN improvement in permeate flux also observed. It was concluded that the use of MCN as a remedy of fouling control will improve the efficiency of membranes considerably. The membrane process are rapid and if the fouling complication are handled properly could be used for the real sample contaminated water in industries.

References

[1] K.J. Choi, S.G. Kim, S.H. Kim, Removal of antibiotics by coagulation and granular activated carbon filtration, J. Hazard. Mater., 151 (2008) 38–43.

[2] D. Zhang, X. Zhang , Z. Meng, Y. Cai, strong adsorption of chlorotetracycline on magnetite nanoparticles, J. Hazard. Mater., 192 (2011) 1088–1093.

[3] K. Kummerer, Antibiotics in the aquatic environment-a review Part I, Chemosphere, 75 (2009) 417–434.

[4] Y. Gao, Y.L.L. Zhang, H. Huang, J. Hu, S.M. Shah, X. Su, Adsorption and removal of tetracycline antibiotics from aqueous solution by graphene oxide, J. Colloid Interface Sci., 368 (2012) 540–546.

[5] S.J. Khan, J.E. Ongerth, Modelling of pharmaceutical residues in Australian sewage by quantities of use and fugacity calculations, Chemosphere, 54 (2004) 355–367.

[6] J. Rivas, A. Encinas, F. Beltran, N, Grahan, Application of advanced oxidation processes to doxycycline and norfloxacin removal from water, J. Environ. Sci. Health A. Tox. Hazard. Subst. Environ. Eng., 46 (2011) 944–951.

[7] A.J. Watkinson, A.J. Murbyd, D.W. Kolpine, S.D. Costanzo, The occurrence of antibiotics in an urban watershed: from wastewater to drinking water, Sci. Total Environ., 407 (2009) 2711–2723.

[8] B. Halling-Sorenson, S.N. Nielsen, P.F. Lanzky, F. Ingerslev, L.U. Holten, H.C. Tzhoft, S.E. Jorgensen, Occurrence, fate and effect of pharmaceutical substances in the environment-a review, Chemosphere, 36 (1998) 357–393.

[9] M. Nelson, A. Dinardo, J. Hochberg, G. Armelagos. Brief communication: Mass spectroscopic characterization of tetracycline in the skeletal remains of an ancient population from Sudanese Nubia 350-550 CE, Am. J. Phys. Anthropol., 143 (2010) 151–154.

[10] C. Bouki, D. Venieri, E. Diamadopoulos, Detection and fate of antibiotic resistant bacteria in wastewater treatment plants, A review, J. Eco. Toxicol. Environ. Saf., 91 (2013) 1–9.

[11] L. Rizzo, C. Manaia, C. Merlin, Urban wastewater treatment plants as hot spots for antibiotic resistant bacteria and genes spread into the environment, A review, Sci. Total. Environ., 447 (2013) 345–360.

[12] Antibiotics in Manure and Soil-A Grave Threat to Human and Animal Health, Policy Paper 43; National Academy of Agriculture Science: New Delhi, India, 20 (2010) 20.

[13] A.L. Batt, D.D. Snow, D.S Aga, Occuurrence of sulfonamide antimicrobial in private water wells in Washington country, Idaho, USA, Chemosphere, 64 (2006) 1963–1971.

[14] M. Jafari, F. seyed, Aghmari, G. Khaghanic, Batch adsorption of cephalosporins antibiotics from aqueous solution by means of multi-walled carbon nanotubes, World Appl. Sci. J., 14 (2011) 1642–1650.

[15] J. Gao, J.A. Pedersen, Adsorption of sulfonamide antimicrobial agents to clay minerals, Environ. Sci. Technol., 39(24) (2005) 9509–9516.

[16] J.W. Peterson, L.J. Petrasky, M.D. Seymourc, R.S. Burkharta, A.B. Schuilinga, Adsorption and breakdown of penicillin antibiotic in the presence of titanium oxide nanoparticles in water, Chemosphere, 87(8) (2012) 911–917.

[17] E.A. Serna-Galvis, J. Silva-Agredo, A.L. Giraldo-Aguirre, O.A. Fl´orez-Acosta, R.A. Torres-Palma, High frequency ultrasound as a selective advanced oxidation process to remove penicillinic antibiotics and eliminate its antimicrobial activity from water, Ultrason. Sonochem., 31 (2016) 276–283.

[18] Y. Liu, X. He, Y. Fu, D.D. Dionysiou, Degradation kinetics and mechanism of oxytetracycline by hydroxyl radical-based advanced oxidation processes, Chem. Eng. J., 284 (2016) 1317–1327.

[19] D. Barlak, F. MostafapourK, Batch equilibrium,kinetics and thermodynamics study of sulfamethaxole antibiotics onto Azolla filiculoides as anovel biosorbent, Br. J. Pharmacol., 13(2) (2016) 1–14.

[20] W. Zhang, G. He, P. Gao, G. Chen, Development and characterization of composite nanofiltration membranes and their application in concentration of antibiotics, Sep. Sci. Technol., 30 (2003) 27–35.

[21] X.D. Zhu, Y.J. Wang , R.J. Sun, D.M. Zhou, Photo catalytic degradation of tetracycline in aqueous solution by nanosized TiO_2, Chemosphere, 92 (2013) 925–932.

[22] D. Balarak, H. Azarpira, Rice husk as a Biosorbent for antibiotic metronidazole removal: Isotherm studies and model validation, Int. J. Chem. Pharma. Tech. Res., 9(7) (2016) 566–573.

[23] R. Ocampo-P´erez, J. Rivera-Utrilla, C. G´omez-Pacheco, M. S´anchez-Polo, J.J. L´opez-Pe˜nalver, Kinetic study of tetracycline adsorption on sludge-derived adsorbents in aqueous phase, Chem. Eng. J., 213 (2012) 88–96.

[24] J.R. Kana, A. Teguia, J. Tchoumboue, Effect of charcoal from Canarium schweinfurthii kernel and from maize cob on the production performances of broiler chickens fed a diet containing peanut cake as main plant protein source, Int. Network for Family Poultry Develop., 19 (2010) 1–52.

[25] H. Li, D. Zhang, X. Han, B. Xing, Adsorption of antibiotic ciprofloxacin on carbon nanotubes; pH dependence and thermodynamics, Chemosphere, 95 (2014) 150–155.

[26] M. Zahoor, Magnetic adsorbent used in combination with ultra filtration membrane for the removal of surfactants from water, Desal. Water Treat., 52 (2014) 3104–3114.

[27] M.M.U. Khattak, M. Zahoor, B. Muhammad, F.A. Khan, R. Ullah, N.M. AbdEI-Salam, Removal of heavy metals from drinking water by magnetic carbon nanostructures prepared from biomass, J. Nanomat., 2017 (2017) 1–10.

[28] M. Zahoor, Removal of pesticides from water using granular activated carbon and ultra filtration membrane a pilot plant study, J. Encap. Adsorption Sci., 3 (2013) 71–76.

[29] L.H. Wu, Nanofiltration membrane-a new separating material and its application in pharmaceutical industry, Membr. Sci. Tech., 17(5) (1997) 11–14.

[30] K.V. Plakas, A.J. Karabelas, Removal of pesticides from water by NF and RO membranes-a review, Desalination, 287 (2012).
[31] K. Kosutic, D. Dolar, D. Ašperger, B. Kunst, Removal of antibiotics from a model wastewater by RO/NF membranes, Sep. Pur. Technol., 53 (2007) 244–249.
[32] M. Zahoor, M. Mahramanlioglu, Adsorption of Imidacloprid on powdered activated carbon and magnetic activated carbon, Chem. Biochem. Eng. Q., 25 (2011) 55–63.
[33] M. Mahramanlioglu, M. Zahoor, M. Kizilcikli, Removal of phenol red by activated and magnetic activated carbon, Fresenius Environ. Bull., 19 (2010) 911–918.
[34] X. Bao, Z. Qiang, J.H. Chang, W. Ben, J. Qu, Synthesis of carbon coated magnetic nanoparticles (Fe_3O_4/C) and its applications for sulfonamide antibiotics removal from water, J. Environ. Sci., 26 (2014) 962–969.
[35] D. Tang, Z. Zheng, K. Lin, J. Zhang, Adsorption of *p*-nitro phenol from aqueous solutions onto activated carbon fiber, J. Hazard. Mater., 143 (2007) 49–56.
[36] M. Moyo, E. Mutare, F. Chigondo, B.C. Nyamunda, Removal of phenol from aqueous solution by adsorption on yeast Saccharomyces cerevisiae, Int. J. Res. Rev. Appl. Sci., 11(3) (2012) 486–494.
[37] T.S. Fasoto, J.O. Arawande, A. Akinnusotu, Adsorption of zinc and chromium ions from aqueous solution onto bagasse, Int. J. Modern Chem., 6(1) (2014) 28–47.
[38] I. Langmuir, The adsorption of gases on plane surfaces of glass, mica and platinum, J. Am. Chem. Soc., 40 (1918) 1361–1403.
[39] H. Freundlich, Uber die adsorption in losungen (adsorption in solution), Z. Phys. Chem., 57 (1906) 384–470.
[40] C. Perk, J.B. Joo, J. Yi, Adsorption of acid dyes using poly electrolyte impregnated mesoporous silica, Korean J. Chem. Eng., 22 (2005) 276–280.
[41] E. Malkoc, Y. Nuhoglu, Determination of kinetic and equilibrium parameters of the batch adsorption of Cr(VI) onto waste corn of Quercus ithaburensis, Chem. Eng. Prog., 46 (2007) 1020–1029.
[42] Y.S. Ho, J.F. Porter, G. Mckay, Equilibrium isotherms studies for the sorption of divalent metal ions onto peat: copper, nickel and lead single component systems, Water Air Soil Pollut., 141 (2002) (2002) 1–33.
[43] A.U. Itodo, H.U. Itodo, Sorption energies estimation using Dubinin-Radushkevich and Temkin adsorption isotherms, Life Sci. J., 7 (2010) 31–39.
[44] S. Lagregren, About the theory of so-called adsorption of soluble substances, Kungliga Svenska Vetenska psaka demiens Handlinga, 24 (1898) 1–39.
[45] Y.S. Ho, G. McKay, Pseudo-second-order model for sorption processes, Process Biochem., 34 (1999) 451–465.
[46] R.C. Dalal, Desorption of phosphate by anion exchange resin, Commun. Soil Sci. Plant Anal., 5 (1974) 531–538.
[47] W.J. Weber, J.C. Morris, Kinetics of adsorption on carbon from solution, journal of sanitary engineering division, J. Amer. Soc. Chem. Eng., 89 (1963) 31–59.
[48] N. Kannan, A. Vanangamudi, A study on removal of chromium VI by adsorption on lignite coal, Indian J. Environ. Prot., 114 (1991) 241–245.
[49] D. Wu, H. Li, S. Liao, X. Sun, H. Peng, D. Zhang, B. Pan, Co-sorption of ofloxacin and Cu(II) in soils before and after organic matter removal, Sci. Total Environ., 481 (2014) 209–216.
[50] C.E. Lin, Y.J. Deng, W.S. Liao, S.W. Sun, W.Y. Lin, C.C. Chem, Electrophoretic behavior and p*Ka* determination of quinolones with a piperazinyl substituent by capillary zone electrophoresis, J. Chrom., 1051 (2004) 283–290.
[51] M. Crespo-Alonso, V.N. Nuruchi, R. Biesuz, G. Alberti, N. Spano, M.I. Pilo, G. Sanna, Biomass against emerging pollution in wastewater: ability of cork for the removal ofloxacin from aqueous solutions at different pH, J. Environ. Chem. Eng., (2013) 1199–1204.
[52] V.V. Goud, K.M. Mohanty, M.S. Rao, N.S Jayakumar, Phenol removal from aqueous solutions using tamarind nut shell activated carbon: batch and column study, Chem. Eng. Technol., 28 (2005) 814–821.
[53] M. Maheshwari, R.K. Vyas, M. Sharma, Kinetics, equilibrium and thermodynamics of ciprofloxacin hydrochloride removal by adsorption on coal fly ash and activated alumina, Desal. Water Treat., 51 (2013) 7241–7254.